J. Cell. Mol. Med. Vol 16, No 7, 2012 pp. 1421-1434

Trivanillic polyphenols with anticancer cytostatic effects through the targeting of multiple kinases and intracellular Ca^{2+} release

Delphine Lamoral-Theys [a], Nathalie Wauthoz [b], Petra Heffeter [c], Véronique Mathieu [d], Utte Jungwirth [c], Florence Lefranc [d, e], Jean Nève [f], Jacques Dubois [a], François Dufrasne [f], Karim Amighi [b], Walter Berger [c], Philippe Gailly [g], Robert Kiss [d, *]

[a] Laboratoire de Chimie BioAnalytique, Toxicologie et Chimie Physique Appliquée, Brussels, Belgium
[b] Laboratoire de Pharmacie Galénique et BioPharmacie, Brussels, Belgium
[c] Department of Medicine I, Institute of Cancer Research, Medical University Vienna, Vienna, Austria
[d] Laboratoire de Toxicologie, Brussels, Belgium
[e] Service de Neurochirurgie, Hôpital Erasme, Université Libre de Bruxelles (ULB), Brussels, Belgium
[f] Laboratoire de Chimie Pharmaceutique Organique, Faculté de Pharmacie, Brussels, Belgium
[g] Laboratoire de Physiologie Cellulaire, Institut des Neurosciences, Université Catholique de Louvain, Brussels, Belgium

Received: March 28, 2011; Accepted: July 26, 2011

Abstract

Cancer cells exhibit de-regulation of multiple cellular signalling pathways and treatments of various types of cancers with polyphenols are promising. We recently reported the synthesis of a series of 33 novel divanillic and trivanillic polyphenols that displayed anticancer activity, at least *in vitro*, through inhibiting various kinases. This study revealed that minor chemical modifications of a trivanillate scaffold could convert cytotoxic compounds into cytostatic ones. Compound **13c**, a tri-chloro derivative of trivanillic ester, displayed marked inhibitory activities against FGF-, VEGF-, EGF- and Src-related kinases, all of which are implicated not only in angiogenesis but also in the biological aggressiveness of various cancer types. The pan-anti-kinase activity of **13c** occurs at less than one-tenth of its mean IC_{50} *in vitro* growth inhibitory concentrations towards a panel of 12 cancer cell lines. Of the 26 kinases for which **13c** inhibited their activity by >75%, eight (*Yes*, *Fyn*, FGF-R1, EGFR, *Btk*, *Mink*, *Ret* and *Itk*) are implicated in control of the actin cytoskeleton organization to varying degrees. Compound **13c** accordingly impaired the typical organization of the actin cytoskeleton in human U373 glioblastoma cells. The pan-anti-kinase activity and actin cytoskeleton organization impairment provoked by **13c** concomitantly occurs with calcium homeostasis impairment but without provoking MDR phenotype activation. All of these anticancer properties enabled **13c** to confer therapeutic benefits *in vivo* in a mouse melanoma pseudometastatic lung model. These data argue in favour of further chemically modifying trivanillates to produce novel and potent anticancer drugs.

Keywords: kinases • polyphenols • cancer • lung • actin cytoskeleton

Introduction

Cancer remains a devastating disease, and the number of cancer-related deaths is increasing worldwide. More than 90% of cancer patients die from tumour metastases because metastatic cancer cells are intrinsically resistant to apoptosis and therefore unresponsive to a large majority of currently available anticancer drugs that induce apoptosis [1, 2]. Many cancer types also display intrinsic resistance to pro-apoptotic stimuli even before metastasizing, such as non-small-cell-lung cancer (NSCLC) [3], melanoma [4], pancreas cancer [5], oesophageal cancer [6] and gliomas [7]. Many cancers further develop acquired chemoresistance during chronic treatments in the shape of the multidrug resistance (MDR) phenotype [8, 9]. One solution to apoptosis resistance and/or the MDR phenotype entails the complementation of cytotoxic

*Correspondence to: Robert KISS, Ph.D.,
Laboratory of Toxicology, Faculty of Pharmacy,
Université Libre de Bruxelles (ULB), CP205/1,
Campus de la Plaine, Boulevard du Triomphe,
1050 Brussels, Belgium.
Tel.: +32-477-62-20-83
Fax: +32-233-25-33-5
E-mail: rkiss@ulb.ac.be

doi:10.1111/j.1582-4934.2011.01403.x

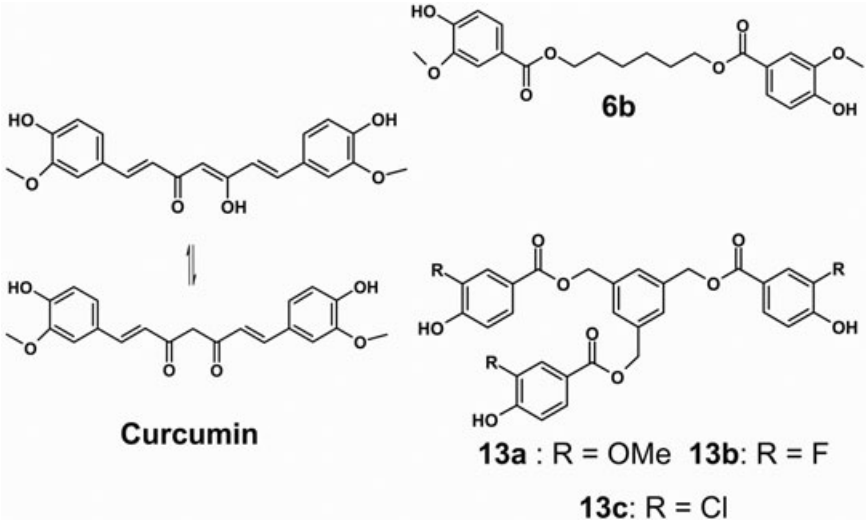

Fig. 1 Chemical structures of the five polyphenolic compounds under study, that is curcumin, **6b**, **13a**, **13b** and **13c**.

therapeutic regimens with cytostatic agents, such as drugs targeting specific protein tyrosine kinases (PTK) or membrane receptors [10]. Kinase inhibitors are the largest class of new anticancer drugs [11], and about 150 kinase inhibitors have been subjected to recent clinical testing, with ~45 kinases listed as primary targets [12]. However, it is already apparent that most cancers can escape from the inhibition of any single kinase [11]. It is thus mandatory to inhibit multiple kinases [11], and partial inhibition of a small number of kinases appears to be a more than promising strategy [10]. Thus, cancer cell resistance to kinase inhibitors and targeted agents, the acquisition of the MDR phenotype and/or the intrinsic resistance to apoptosis altogether prevent effective cancer treatment.

As single compounds, some polyphenols can potentially target multiple kinases implicated in cancer cell biology, in addition to the multiple anticancer effects already reported for polyphenols such as anti-oxidative, pro-apoptotic, DNA damaging, anti-angiogenic and immunostimulatory effects [13]. Examples include curcumin [14], resveratrol [15] and the green tea polyphenol epigallocatechin-3-gallate (EGCG) [16]. Finally, some polyphenols also appear to exert their cytotoxic anticancer activities through the impairment of calcium homeostasis [17–19].

This study sought to further characterize the anticancer activities of synthetic divanillic and trivanillic polyphenols (Fig. 1), for which preliminary anticancer pharmacological properties have recently been reported in addition to proven anti-kinase activity against *Aurora* and *Wee1* kinases [2]. The *in vitro* 50% growth inhibitory concentrations (IC_{50}) of these compounds were first determined in 11 human and one mouse cancer cell lines. We then investigated whether these synthetic polyphenols along with curcumin (a reference compound) display cytostatic or cytotoxic effects at their respective IC_{50}s. The obtained data prompted us to characterize the effects of the synthetic trivanillates in terms of apoptotic features, cell cycle kinetics, anti-kinase activity and $[Ca^{2+}]_i$ modifications. Compound **13c** (Fig. 1) emerged as a hit, and its anticancer activity was therefore further characterized in terms of modifying actin cytoskeleton organization and MDR-related substrate activity. Finally, compound **13c** was assayed *in vivo* in the B16F10 melanoma metastatic lung model [20] through inhalation procedures that we recently validated for temozolomide [21], an alkylating agent that displays significant anticancer activity against apoptosis-resistant cancers [22].

Materials and methods

Materials

The compounds under study (**6b**, **13a**, **13b**, **13c** and curcumin; Fig. 1) were synthesized in our laboratory facilities as detailed elsewhere [2]. The Krebs solution for $[Ca^{2+}]_i/[Ca^{2+}]_{ER}$ measurements contained the following components (mM): 135 NaCl, 5.9 KCl, 1.8 $CaCl_2$, 1.2 $MgCl_2$, 11.6 HEPES and 10 glucose (pH 7.4). In the Ca^{2+}-free solution, $CaCl_2$ was omitted and 0.2 mM EGTA was added. Thapsigargin, histamine and ionomycin were purchased from Sigma-Aldrich (Bornem, Belgium). Fura-2/AM was obtained from Molecular Probes (Invitrogen, Merelbeke, Belgium).

Cell cultures for the determination of IC_{50} growth inhibition concentrations

We used one mouse and 11 human cancer cell lines that were obtained from the European Collection of Cell Culture (ECACC, Salisbury, UK), the American Type Culture Collection (ATCC, Manassas, VA, USA) and the Deutsche Sammlung von Mikroorganismen und Zellkulturen (DSMZ, Braunschweig, Germany). The origin of each cell line is detailed in the legend to Table 1. We have also made use of two primocultures of human

Table 1 Determination of *in vitro* anticancer activity in 11 human and one (B16F10) mouse cancer cell lines

Compounds	*In vitro* IC_{50} growth inhibitory values (μM; ≥100 μM)*, †												
	U373	T98G	Hs683	LoVo	A549	MCF-7	PC-3	OE21	OE33	VM21	VM48	B16F10	Mean ± S.E.M.
6b	22	56	63	34	27	39	39	68	63	71	56	22	47 ± 5
13a	28	28	27	29	23	55	30	16	19	37	35	41	31 ± 3
13b	37	37	25	48	26	41	44	73	71	65	61	31	47 ± 5
13c	31	25	31	33	26	33	36	28	40	35	32	7	30 ± 2
Curcumin	18	25	22	24	27	24	33	27	35	33	33	10	26 ± 2

*The IC_{50} values were determined by means of the MTT colorimetric assay. The cell lines include human U373 (ECACC code 89081403), T98G (ATCC code CRL1690) and Hs683 (ATCC code HTB-138) glioblastoma; LoVo (DSMZ code ACC350) colon cancer; A549 (DSMZ code ACC107) NSCLC; MCF-7 (DSMZ code ACC115) breast cancer; PC-3 (DSMZ code ACC465) prostate cancer; OE21 (ECACC code 96062201) and OE33 (ECACC code 96070808) esophageal cancer; and VM21 and VM48 melanoma primocultures detailed in Refs. [24, 40]. The mouse B16F10 melanoma cell line was obtained from ATCC (code CRL-6475).

†Part of the data reported in Table 1 was already published in Ref. [2].

melanoma, VM21 and VM48 [23]. The cancer cell lines under study were cultured in RPMI medium (Invitrogen) supplemented with 10% heat-inactivated foetal calf serum (Invitrogen), 4 mM glutamine, 100 μg/ml gentamicin and penicillin–streptomycin (200 U/ml and 200 μg/ml, respectively) (Invitrogen).

Cell cultures were frequently checked for *Mycoplasma* contamination (PCR-ELISA, Boehringer, Mannheim).

Determination of IC_{50} growth inhibition concentration

The overall growth level of each human cancer cell line was determined using the colorimetric MTT (3-[4,5-dimethylthiazol-2yl])-diphenyl tetrazolium bromide; Sigma-Aldrich) assay as detailed and validated previously [2, 23]. Each experimental condition was evaluated in sextuplicate.

MDR cell cultures

Cell culture

Human cell lines and their chemoresistant sublines used in this study were obtained as follows. The head and neck squamous carcinoma cell line KB-3-1 and its Pgp overexpressing subline KBC-1 [24, 25] were generously donated by Dr. D.W. Shen (Bethesda, MD, USA). The KB-3-1 derivative KB-HU selected against hydroxyurea [26] was generously donated by Dr. Y.C. Cheng (Yale University, New Haven, CT, USA). The small cell lung carcinoma cell line GLC-4 and its MRP1 and LRP overexpressing adriamycin-resistant subline GLC-4/$_{ADR}$ [25, 27] were generously donated by Dr. E.G. deVries (Groningen, The Netherlands). The human colon cancer cell line HCT116 p53-wild-type and its p53 (−/−) clone with deleted p53 [28] were generously donated by Dr. B. Vogelstein (John Hopkins University, Baltimore, USA). The mesothelioma cell model P31 and its respective cis-platin-resistant subline P31/*cis* [29] were generously donated by Dr. K. Grankvist (Umeå University, Umeå, Sweden). The chemosensitive chronic myeloid leukaemia K562S cell line and its daunorubicin-resistant subline K562R [30] were generously donated by Dr. S. Yanovich (Medical College of Virginia, VA, USA). Immunoblotting validation of overexpressed ABC transporters and p53 deletion are available upon request. All cell lines were cultured in RPMI1640 medium supplemented with 10% foetal bovine serum with the exception of HCT116 cells (grown in McCoy's medium) and P31 cells (grown in Eagle's minimal essential medium). In case of the resistant sublines, the respective selection drug was frequently added, as published. Cell cultures were frequently checked for *Mycoplasma* contamination (PCR-ELISA).

Cell viability assays

Cells (2×10^3) in 100 μl were plated into individual wells in 96-well plates and allowed to attach for 24 hrs. Drugs in appropriate concentration ranges were added to the wells in another 100 μl of growth medium, and cells were exposed for 72 hrs. The proportion of viable cells was then determined by the MTT colorimetric assay as detailed in the previous section.

Quantitative videomicroscopy

The investigation of whether curcumin and compounds **6b**, **13a**, **13b** and **13c** displayed cytotoxic *versus* cytostatic effects was conducted by means of computer-assisted phase contrast microscopy (quantitative videomicroscopy) in human U373 glioblastoma and A549 NSCLC cell lines as detailed elsewhere [2, 31]. U373 cells were monitored for 72 hrs in the absence (control) or the presence of 20 μM curcumin, 20 μM **6b**, 30 μM **13a**, 30 μM **13c** and 40 μM **13b**, which represent the approximate IC_{50} of each compound (Table 1) as calculated by means of the MTT colorimetric assay described earlier. A549 cells were monitored at 30 μM concentrations for curcumin and **6b** and 25 μM concentrations for **13a**, **13b** and **13c**. Movies were built on the obtained time-lapse image sequences, which enabled a detailed screening for cell viability to determine whether the compound under study induced cytostatic *versus* cytotoxic effects [2, 31]. All experimental conditions were performed in triplicate.

Determination of apoptotic death features and cell cycle kinetics

Apoptotic rates and cell cycle kinetic analyses in U373 and A549 cells either untreated (control) or treated for 48 and 72 hrs with 20 μM concentrations of compounds **13a**, **13b** and **13c** and curcumin were concomitantly determined using flow cytometry after TUNEL and propidium iodide staining as detailed previously [20]. Briefly, cancer cells were harvested by trypsinization, fixed in paraformaldehyde 1% during 1 hr at room temperature followed by incubation in ethanol 70% overnight at −20°C. Cancer cells (1×10^6 cells) from each sample were then stained with the APO-Direct™ kit (BD Pharmingen, Erembodegem, Belgium) following the manufacturer's recommandations: FITC-dUTPs were added to the apoptotic DNA breaks by incubation with TdT enzyme during 1 hr at 37°C. After two washes, cells were incubated in propidium iodide staining solution for 30 min. at room temperature in presence of RNAse. Fluorescence was immediately analysed after on a Cell Lab Quanta flow cytometer (Beckman Coulter Analis, Suarlee, Belgium). Each condition was evaluated in triplicate.

Determination of mitotic rates and mitotic duration

Cells undergoing division exhibited very bright patterns compared to non-dividing cells (Fig. 3). Based on this observation, we developed a custom division detection system capable of identifying cells undergoing division using time-lapse sequences. This detection method is based on automatic event detection completed by an interactive validation/correction procedure as previously described [32]. At the end of the sequence analysis, all events are linked to different cell divisions, making available the number of cell divisions as well as their durations [32]. We computed the cell division numbers normalized by the number of cells that were counted in the first frame.

The total number of mitoses and mitosis duration were determined in U373 and A549 cells treated for 72 hrs with 20 μM compound **13c**. Each experimental condition was evaluated in triplicate.

Analyses of actin cytoskeleton organization

U373 glioblastoma cells were cultured on glass cover slips to approximately 50% confluence to permit the analyses of individual cells as previously described [31]. Fluorescent phallacidin conjugated with Alexa Fluor 488 (Molecular Probes, Invitrogen) was used to label fibrillar actin, whereas Fluor 594-conjugated DNAseI (Molecular Probes, Invitrogen) was used to stain globular actin as previously described [31]. Cover slips were mounted on microscope slides with 10 μl Moviol agent (Calbiochem, VWR, Heverlee, Belgium). Pictures were obtained using a 40× microscope oil-immersion objective (Zeiss observer.Z1, Zeiss, Oberkochen, Germany) and an Axiocam HRm Zeiss camera controlled by software. Pictures were converted to stacks and navigated using the Axiovision Rel 4.6 software. Three cover slips were analysed, and three pictures were taken for each cover slip (with the same exposure time) for each condition. The most representative images are shown.

Intracellular calcium concentration ($[Ca^{2+}]_i$) measurements

$[Ca^{2+}]_i$ measurements

Cells were loaded with 1 μM Fura-2/AM for 60 min. at room temperature. Fura-2-loaded cells were alternatively excited at 340 and 380 nm, and fluorescence emission was monitored at 510 nm using a Deltascan spectrofluorimeter [Photon Technology International (PhotoMed, Seefeld, Germany), dichroic mirror at 400 nm] coupled to an inverted microscope [Nikon Diaphot (Surrey, England), oil immersion objective 40× N.A. 1.3]. Fluorescence intensity was recorded over the entire surface of single cells. $[Ca^{2+}]_i$ was calculated from the ratio of the fluorescence intensities at the two wavelengths using an intracellular calibration procedure performed after cell permeabilization with 5 μM ionomycin [33].

$[Ca^{2+}]_{ER}$ measurements

To perform $[Ca^{2+}]_{ER}$ measurements, we used Cameleon probe D1ER kindly provided by Dr. R. Tsien [34, 35]. Cameleon D1ER was transfected into U373 cells with Lipofectamine 2000 reagent according to the manufacturer's instructions (Invitrogen, Carlsbad, CA, USA). Cells were plated on glass cover slips, and 72 hrs after transfection, they were mounted on a Zeiss Axiovert S-100 microscope (Zeiss). Images were acquired every 30 sec. for 40 min. with a Zeiss Axiocam camera and analysed by the Zeiss AxioVision software. Emission ratio imaging was accomplished using a 435 nm excitation filter and two emission filters (485 and 535 nm) controlled by a filter wheel (Ludle).

Kinase activity determination

We originally provided ProQinase (Freiburg, Germany) with compounds **6b**, **13a**, **13b** and **13c** as stock solutions in 100% DMSO, and aliquots were further diluted with water in 96-well microtitre plates directly before use. For each kinase assay, 5 μl from a 2×10^5 M/10% DMSO compound solution was transferred to the assay plates. The final volume of the assay was 50 μl. The final assay concentration for each compound was 2 μM.

A radiometric protein kinase assay (^{33}PanQinase® Activity Assay) was used for measuring the kinase activity of the 256 protein kinases under study as detailed previously [2].

In vivo B16F10-related experiments

All animal experiments used female B6D2F1 mice (18–22 g; Charles Rivers, Arbresle, France) and were performed on the basis of authorization no. LA 1230568 from the Animal Ethics Committee of the Federal Department of Health, Nutritional Safety, and the Environment (Belgium).

We first determined the maximal tolerated dose (MTD) for compound **13c** through inhalation procedures. MTD was defined in this study as the concentration in one endotracheal single dose causing no death in a group of three healthy mice (*i.e.* not grafted with tumours). The survival period and weight of the animals were recorded for up to 21 days post-administration. Five different doses (5, 10, 20, 40 and 80 mg/kg bw) were used for determination of the MTD index. A pulmonary delivery device was used to administer the different doses; the volume administered was 50 μl of the

inhalation suspension consisting of 0.2%, 0.4%, 0.8%, 1.6% or 3.2% compound **13c**. The MTD appeared to be 40 mg/kg for compound **13c**.

B16F10 melanoma pulmonary pseudo metastases were obtained by the i.v. (lateral tail vein) administration of 2.5×10^5 B16F10 cells (200 μl), as we detailed previously [20, 21]. All mice were grafted with B16F10 tumour cells on the same day. Mice were randomized on the fourth day post-tumour grafting, and treatments began on the fifth day post-tumour grafting. Each experimental group included 11 mice.

Compound **13c** (40 mg/kg) was administered directly to the lungs [50 μl of the inhalation suspension for inhalation, 1.6% compound **13c** (m/v) by the endotracheal route] three times (Monday, Wednesday and Friday) a week for three consecutive weeks. Mouse survival was checked at 9:00 a.m. and 4:00 p.m. each day. Mouse weight was recorded three times per week (Monday, Wednesday and Friday). Each B16F10 melanoma-bearing mouse was sacrificed (by cervical dislocation) when it had lost 20% of its weight compared to that determined at the time of the tumour graft or if it was suffocating. The lungs were removed, fixed in buffered formalin, paraffin-embedded and then processed for conventional histopathological analyses.

Statistics

Statistical comparisons between paired groups were established by performing the non-parametric Mann–Whitney test. Student's *t*-tests and χ^2-tests were used to determine statistical significance for $[Ca^{2+}]_i/[Ca^{2+}]_{ER}$ measurements. Survival analyses were performed by means of Kaplan–Meier curves, which were compared with the log-rank test. All statistical analyses were realized using Statistica (Statsoft, Tulsa, OK, USA).

Results

Table 1 shows that curcumin and compounds **6b**, **13a**, **13b** and **13c** displayed similar *in vitro* growth inhibitory patterns in 11 human and one mouse (B16F10 melanoma) cancer cell lines.

Figure 2 clearly indicates that curcumin and **13a** displayed cytotoxic effects, while **6b** (Fig. SI-1), **13b** and **13c** displayed cytostatic properties in the human U373 glioblastoma cell line. Thus, similar IC_{50} values (as revealed in Table 1) led to markedly distinct mechanisms of action in a given cancer cell line. Each compound was evaluated here at a concentration close to its IC_{50} in U373 cells.

Although the cytotoxic effects of curcumin as revealed by quantitative videomicroscopy directly translate into marked pro-apoptotic features as revealed by TUNEL staining (Fig. 3A and B), this is not the case with respect to **13a**, which displayed cytotoxic effects (Fig. 2) relating to non-apoptotic cell death (Fig. 3A and B). As expected from the quantitative videomicroscopy analyses, **13b** and **13c** induced weak pro-apoptotic effects (Fig. 3A and B).

Compounds **13a**, **13b** and **13c** only weakly modified cell cycle kinetic parameters in U373 and A549 cells as revealed by PI-staining relating to the determination of cancer cells in either the G1 (Fig. 3C) or G2 (Fig. 3D) phase of the cell cycle. We thus utilized quantitative videomicroscopy analyses to investigate whether compounds **13b** and **13c**, which are cytostatic, could impair mitosis. Figure 3Ea–Ec illustrate the morphological patterns of two

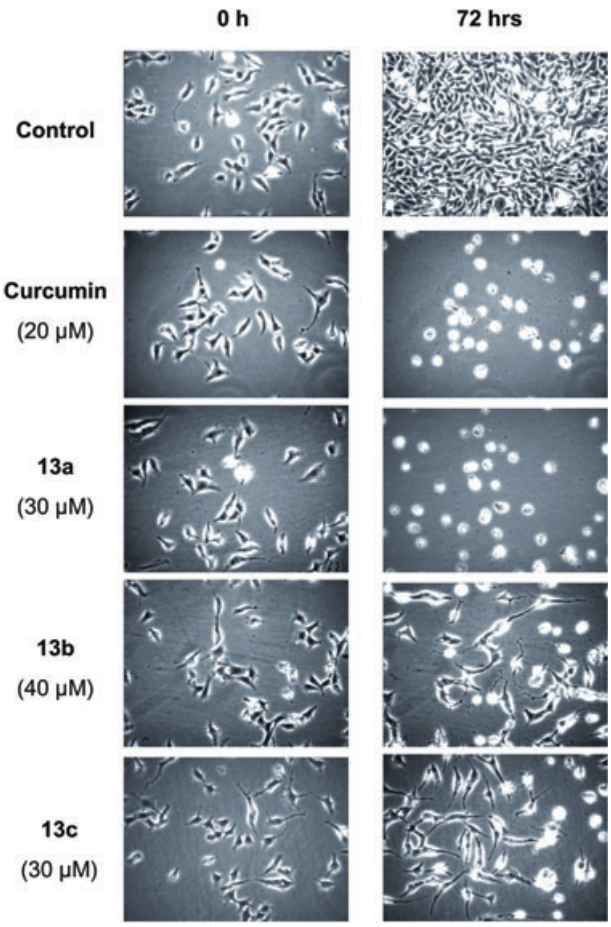

Fig. 2 Morphological illustrations of the cytostatic *versus* cytotoxic effects provoked by curcumin, **13a**, **13b** and **13c** on U373 cells. The images were recorded and digitized by means of computer-assisted phase-contrast microscopy (quantitative videomicroscopy) at a G×200 magnification.

U373 cells (C1 and C2), with C1 entering mitosis as revealed by the white halo under the cell (Fig. 3Ea) and then these C1 cell completing mitosis (Fig. 3Eb), giving birth to two daughter cells (D1C1 and D2C1; Fig. 3Ec). The software we developed [32] enables the number of mitoses as well as mitosis duration to be computed for each experimental condition (performed in triplicate) from the 1080 images digitized every 4 min. for 72 hrs by means of quantitative videomicroscopy. Figure 3Fa shows that compounds **13b** and **13c** markedly decreased the mitosis numbers in the U373 cell line. We did not evaluate compound **13a** because it is cytotoxic (Fig. 2). Figure 3Fb further reveals that decreases in mitosis numbers (Fig. 3Fa) were paralleled by increases in mitosis duration.

The cytostatic effects of **13b** and **13c** (Fig. 2), paralleled by their effects on mitosis (Fig. 3) and our preliminary data revealing that several of the divanillates (including **6b**) and trivanillates (**13a**, **13b** and **13c**) displayed anti-*Aurora* and anti-*Wee1* kinase activity [2] prompted us to characterize the anti-kinase profiles of **13a**,

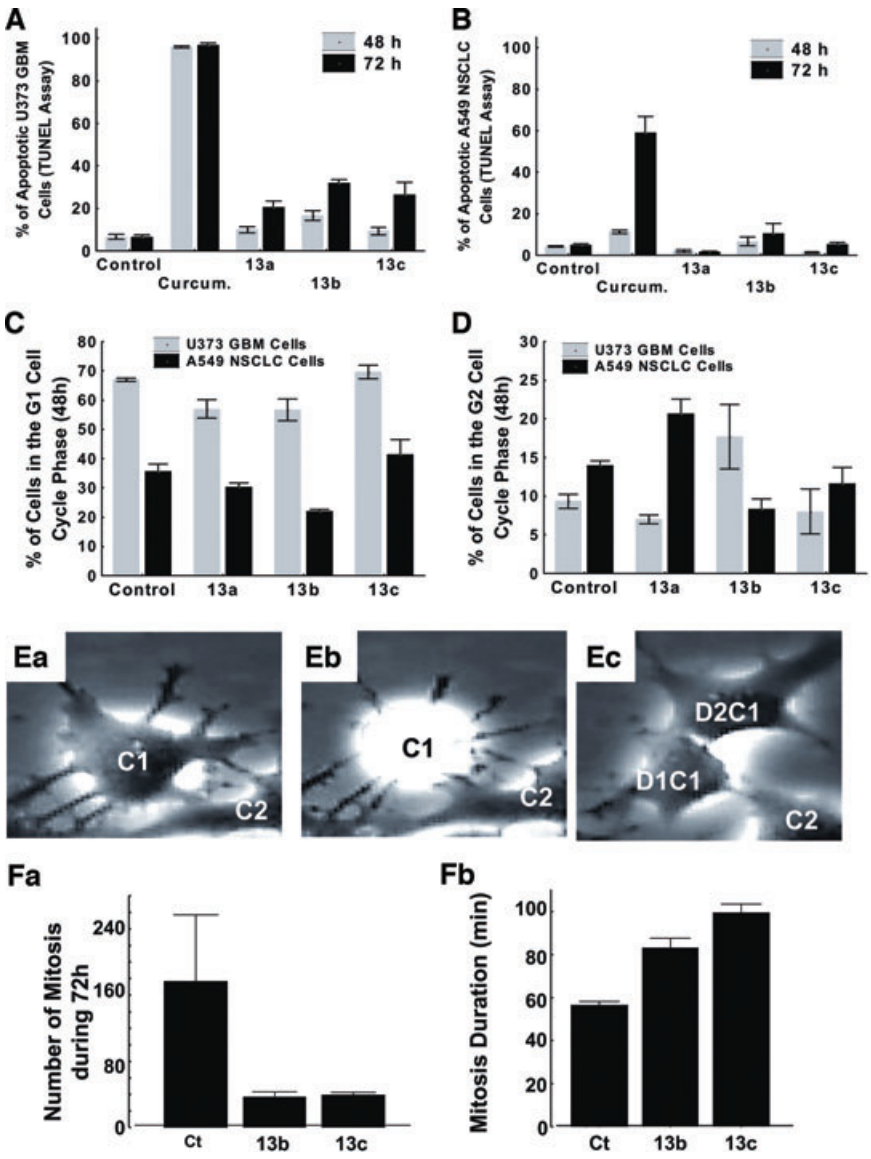

Fig. 3 Determination of compound-induced effects on apoptotic, cell cycle kinetic and mitotic characteristics of human cancer cells. Determination of the percentages of U373 (**A**) and A549 (**B**) cells undergoing apoptosis after 48 hrs *versus* 72 hrs of treatment with 20 μM curcumin, **13a**, **13b** and **13c**. Determination of the percentages of U373 (**A**) and A549 (**B**) cells in the G1 (**C**) and G2 (**D**) phases of the cell cycle after 72 hrs of treatment with 20 μM curcumin, **13a**, **13b** and **13c**. (**Ea–Ec**) Morphological illustrations of a mitosis monitored through computer-assisted phase-contrast microscopy (G×1400). (**Ea**–**Ec**) The morphological patterns of two cells (C1 and C2), with C1 entering mitosis as revealed by the white halo under C1 (Fig. 3Ea) and C1 completing mitosis (Fig. 3Eb), giving birth to two daughter cells (D1C1 and D2C1; Fig. 3Ec). Number (**Fa**) and duration (**Fb**) of mitoses in U373 cells treated for 72 hrs with 20 μM **13b** and **13c**. The data in (**A–D**) and (**Fa**–**Fb**) are presented as means ± S.E.M. values calculated on three independent experimental values.

13b and **13c** using a panel of 256 kinases (Table SI-1). Figure 4 shows that **13c** decreased the residual activity of 26/256 kinases by >75%, including various mutated forms of the EGFR and *Flt3* kinases. These effects were observed at a concentration of 2 μM that represents ~5% of the IC_{50} (Table 1). In sharp contrast, compound **13b** (Fig. 4) only weakly inhibited kinase activity, while compound **13a** (Fig. 4) failed to inhibit kinase activity at 2 μM.

Compound **13c** is cytostatic (Fig. 2) and impairs mitosis (Fig. 3), and of the 26 kinases for which **13c** inhibited their activities by >75% (Fig. 4), eight (*Yes*, *Fyn*, FGF-R1, EGFR, *Btk*, *Mink*, *Ret* and *Itk*) are implicated in control of the actin cytoskeleton organization to some degree. In addition, 2 μM **13c** further decreased the activity of an additional set of six kinases (*Kit*, *Pak3*, *Apha3*, *Syk*, *Erk6* and PKA) that are also implicated in the control of the actin cytoskeleton by 50–75%. These data prompted us to investigate **13c**-mediated effects on the actin cytoskeleton. Figure 5Aa illustrates the typical organization of the actin cytoskeleton in U373 cells cultured for 24 hrs on glass cover slips and left untreated. Fibrillar actin appears in green, while globular actin appears in red. Figure 5Ab illustrates at a higher magnification the presence of multiple stress actin fibres located at the lamellipodia and filopodia of these untreated U373 cells (indicated by the thin white arrows) as well as the presence of rare areas with condensed fibrillar actin (indicated by the thick white arrows).

Treatment of U373 cells for 24 hrs with 20 μM **6b** did not apparently modify the U373 actin cytoskeleton (Fig. 5B). In sharp

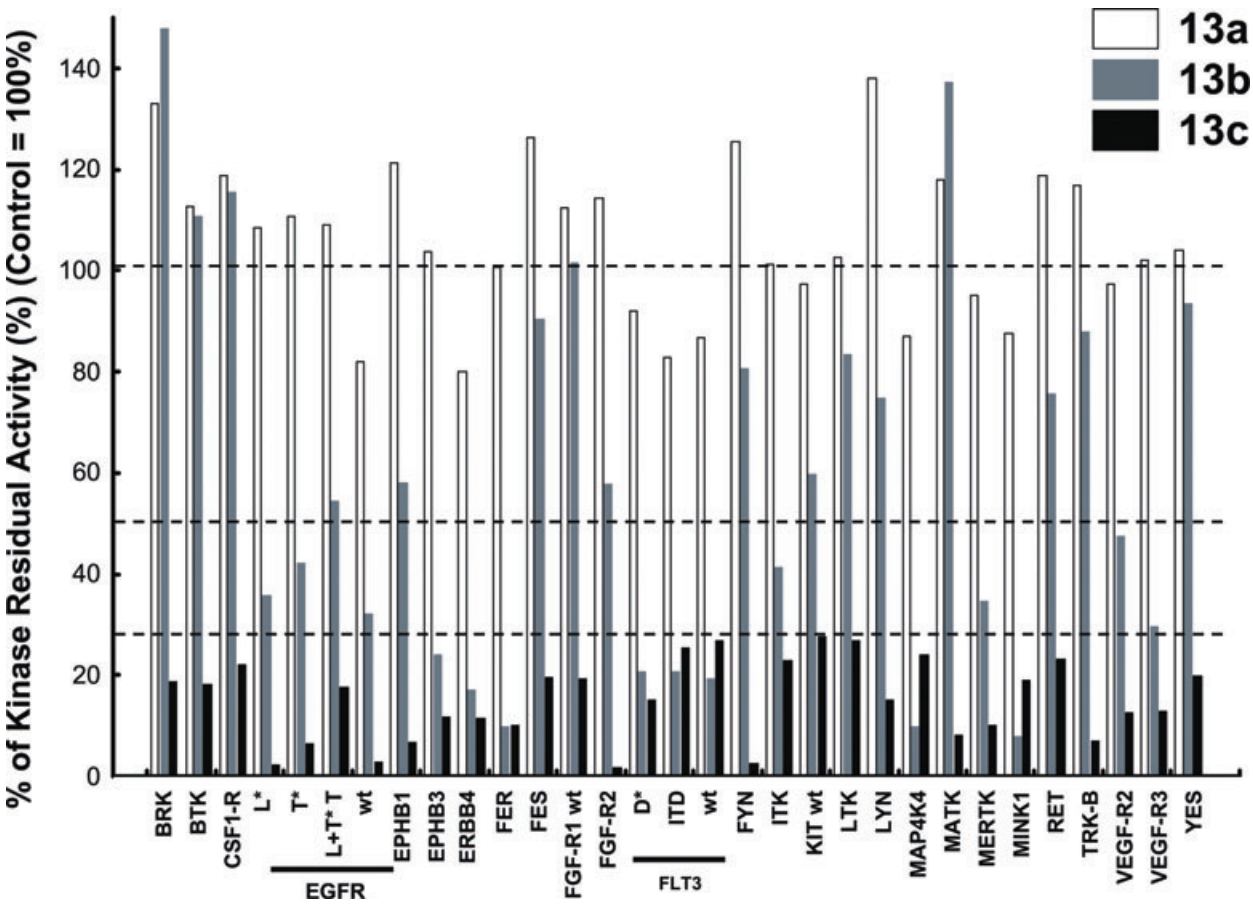

Fig. 4 Characterization of trivanillate-induced anti-kinase activity. Percentage of residual activity for 26 out of the 256 kinases (listed in Table S1) for 2 μM **13a**, **13b** and **13c**. EGFR was assayed as its wild-type (wt) form as well as its L858R (L*), T790M (T*) and L858R + T790M (LT) forms. In the same manner, FLT3 was assayed as its wt form as well as its D835Y (D*) and ITD mutated forms.

contrast, one-tenth of this concentration, 2 μM, of compound **13c** eliminated the stress actin fibres located in the lamellipodia and filopodia and markedly increased the areas of dense fibrillar actin (Fig. 5Ca and Cb).

Modifications in actin cytoskeleton organization can occur not only through the targeting of specific clusters of kinases but also through modifications in $[Ca^{2+}]_i$. Compounds **13a**, **13b** and **13c** were assayed at 20 μM (Fig. 6A and B) in the presence (Fig. 6B) or absence of extracellular Ca^{2+} concentrations (Fig. SI-2) and then at 2 μM (Fig. 6C) for their ability to modify $[Ca^{2+}]_i$ in U373 cells. As shown in Figure 6A and B, treatment of U373 cells for 30 min. with 20 μM **13b** produced a rapid but transient increase in $[Ca^{2+}]_i$ that almost reached 400 nM after 5 min. and then decreased to a steady level of about 150 nM. A significant increase in $[Ca^{2+}]_i$ was already obtained at 2 μM (Fig. 6C), which is much lower than the IC_{50} (Table 1). An increase in $[Ca^{2+}]_i$ was also observed after treatment of the cells with 20 μM **13c**, but the response was slower, reaching a plateau value of about 200 nM after 15 min. of treatment (Fig. 6A and B). For **13a**, the effect observed was much weaker than that for **13b** and **13c** and was absent at a concentration of 2 μM (Fig. 6A and B). Interestingly, the effects of the three compounds were similar in the absence of extracellular Ca^{2+} (Fig. SI-2), suggesting that they induced a release of Ca^{2+} from internal stores. We therefore measured their effects on the intrareticular concentration of Ca^{2+} ($[Ca^{2+}]_{ER}$). As expected, we observed that **13b** induced a rapid decrease of $[Ca^{2+}]_{ER}$ (Fig. 6D), explaining the rapid increase of $[Ca^{2+}]_i$ (Fig. 6A). Compounds **13c** and **13a** also affected $[Ca^{2+}]_{ER}$, but their effects were slower and much smaller than that of **13b** (Fig. 6D). We confirmed these observations by measuring the response of U373 cells to 100 μM histamine, an agonist known to induce an IP_3-mediated release of Ca^{2+}. After a 25-min. treatment with 20 μM **13a**, the response to histamine was still present (5/5 experiments; Fig. 6A). As expected, this response was abolished after treatment with 20 μM **13b** or **13c** (4/6 experiments for each compound; significantly different from **13a** treatment, χ^2-test < 0.05).

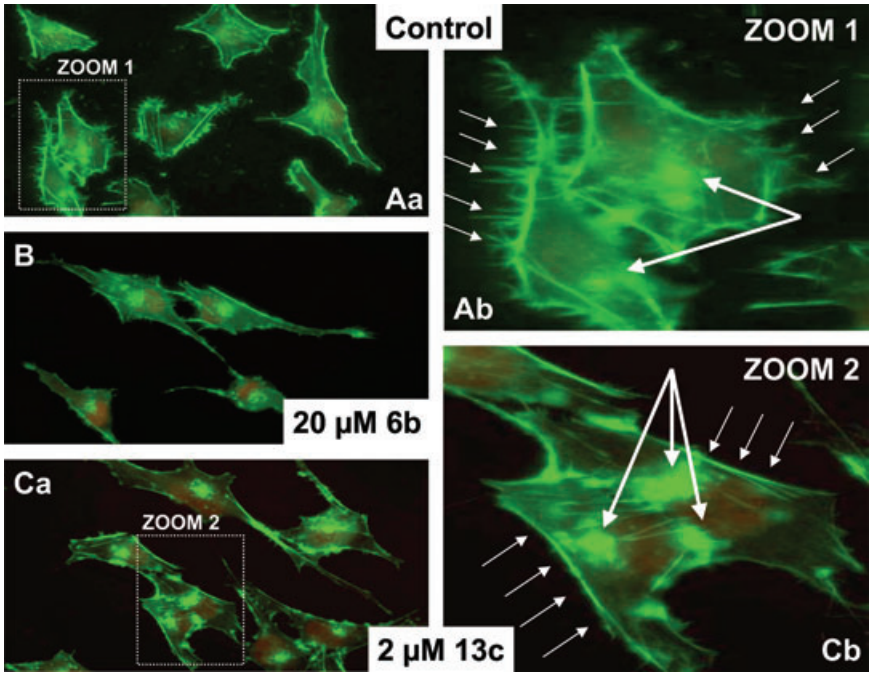

Fig. 5 Fluorescence microscopy-related illustrations of actin cytoskeleton organization in U373 cells (G×1400). U373 cells that were left untreated (control; **Aa** and **Ab**) or treated for 24 hrs with 20 μM **6b** (**B**) or 2 μM **13c** (**Ca** and **Cb**). The thin white arrows in control U373 cells (**Ab**) point to stress actin fibres, which disappear when the U373 cells are treated with 2 μM **13c** (**Cb**). The thick white arrows in **13c**-treated U373 cells (**Cb**) point to the emergence of large areas of polymerized actin, which are much less pronounced in control U373 cells (**Ab**).

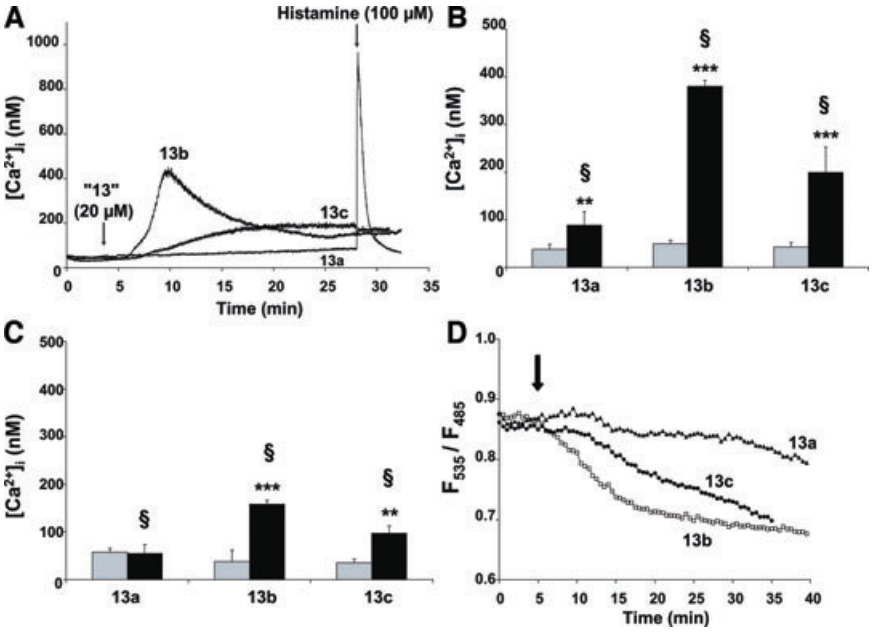

Fig. 6 Effects of **13a**, **13b** and **13c** compounds on cytosolic ($[Ca^{2+}]_i$) and intrareticular ($[Ca^{2+}]_{ER}$) of free Ca^{2+}. (**A**) Time course of $[Ca^{2+}]_i$ when U373 cells were treated with the '**13**' compounds (left arrow) and then stimulated with 100 μM histamine (right arrow). (**B**, **C**) Quantification of the resting $[Ca^{2+}]_i$ (grey columns) and the peak of $[Ca^{2+}]_i$ (black columns) obtained after treatment of the cells with 20 μM (**B**) or 2 μM (**C**) of each drug. (**D**) Evolution of the $[Ca^{2+}]_{ER}$ when U373 cells were treated with 20 μM **13a**, **13b** and **13c** compounds. Data presented are the means of the values measured on five cells transfected with Cameleon D1ER and are representative of at least three independent experiments (different cultures and transfections). ** and *** indicate significantly different from non-stimulated resting $[Ca^{2+}]_i$ (Student's *t*-test, $P < 0.01$ and $P < 0.001$, respectively; $n = 5–6$); §: different from other '**13**' compounds (ANOVA followed by multiple comparison with Student–Newman–Keuls method).

We then wanted to investigate as whether MDR cancer cells can resist **13c** treatments. K562-R cancer cells (Fig. 7A), which markedly overexpress Pgp pumps [36], were significantly resistant to doxorubicin compared to K562-S cells (Fig. 7A), while compound **13c** displayed similar growth inhibitory effects in K562-S and K562-R cancer cells (Fig. 7B). In the same manner, KBC-1 cancer cells, which also markedly overexpress Pgp pumps [36] and were significantly resistant to vinblastine compared to KB-3-1 cancer cells (Fig. 7C), do not resist **13c** (Fig. 7D). Hydroxyurea-sensitive (KB-3-1; Fig. 7E) and hydroxyurea-resistant (KB-HU; Fig. 7E) KB cells displayed similar growth inhibition sensitivity to **13c** (Fig. 7F). KB-HU cells are drug resistant due to ribonucleotide

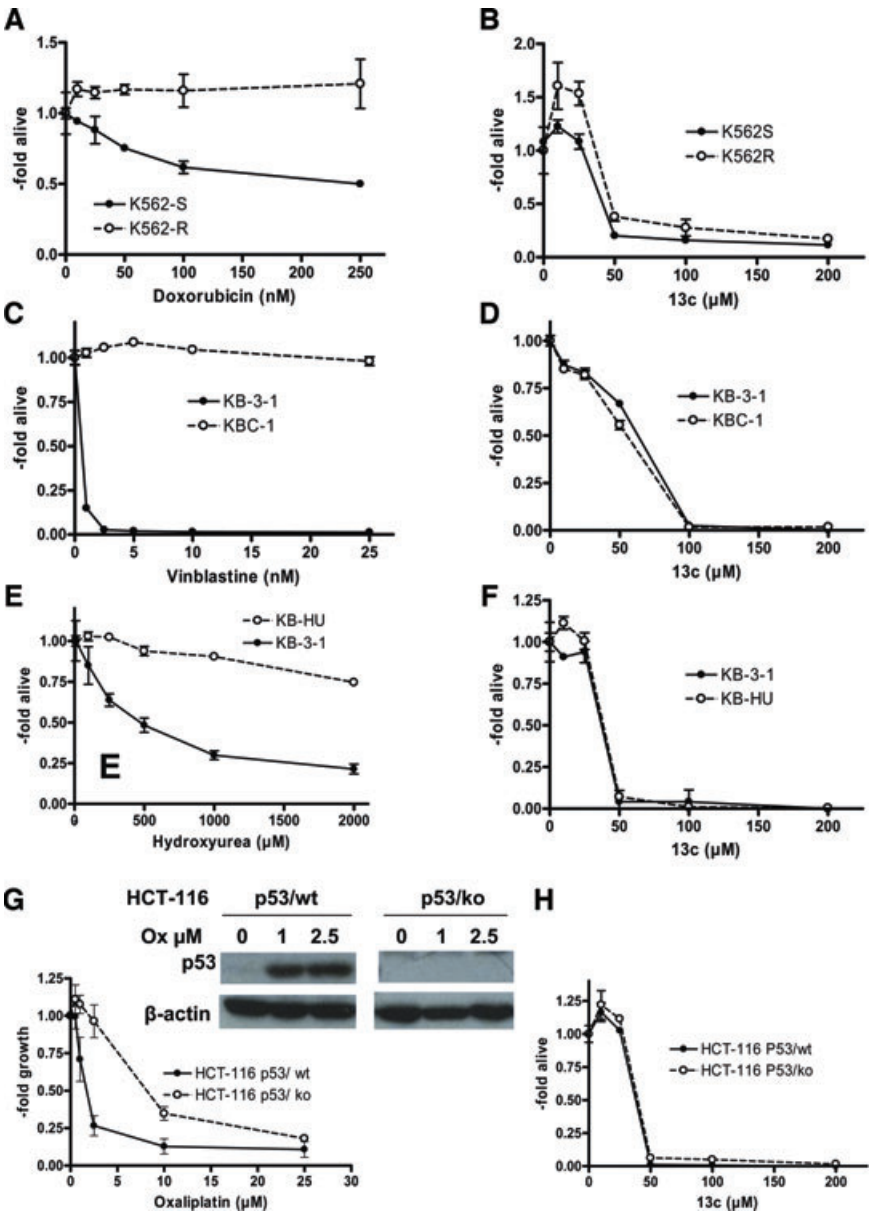

Fig. 7 Characterization of the *in vitro* anticancer activity of **13c** in various MDR cancer cell lines. The anticancer activity of **13c** was assayed in five distinct MDR cancer cell lines and one cancer cell line that has been knocked down for p53. The five MDR cancer cell lines included the doxorubicin-sensitive and doxorubicin-resistant K562 chronic myeloid leukemia cells (**A**, **B**), the chemosensitive *versus* vinblastine-resistant (**C**, **D**) and hydroxyurea-resistant (**E**, **F**) resistant KB-3-1 head and neck squamous carcinoma cells. The wild-type (wt) *versus* p53 knock out (ko) colon cancer cells were challenged with oxaliplatin (**G**) and **13c** (**H**), and a Western blot control was also provided with respect to p53 protein expression in the sublines.

reductase overexpression. The same features were also observed in GLC-4 lung cancer cells in terms of sensitivity (GLC-4; Fig. SI-3A) and resistance (GLC-4/adr; Fig. SI-3A) to adriamycin when tested with **13c** (Fig. SI-3B) and with mesothelioma P31 cells in terms of sensitivity (P31wt; Fig. SI-3C) and resistance (P31cis; Fig. SI-3C) to cisplatin when tested with **13c** (Fig. SI-3D). GLC-4 adriamycin-resistant cells overexpress the MDR-associated protein-1 (MRP1, a ABCC1 efflux pump) and lung-related protein (LRP), while the mechanisms conferring resistance to cisplatin in P31cis cells remain unknown. Altogether, these data suggest on the one hand that compound **13c** is not a substrate for MDR-related pumps and on the other hand that compound **13c** is active against several (multi-drug) resistant cell models.

Apart from clear evidence of **13c**-related efficiency in inhibiting the growth of MDR cancer cells, **13c** is also active in apoptosis-resistant cancer cells. Indeed, wild-type HCT-116 overexpressed p53 after challenge with oxaliplatin, a feature that was not observed in HCT-116 $p53^{-/-}$ KO cells (Fig. 7G). HCT-116 $p53^{-/-}$ cancer cells accordingly developed significant levels of resistance to oxaliplatin (Fig. 7G). Compound **13c** displayed similar *in vitro* growth inhibitory effects in wild-type and $p53^{-/-}$ HCT-116 cells (Fig. 7H). This indicates that the anticancer activity of compound

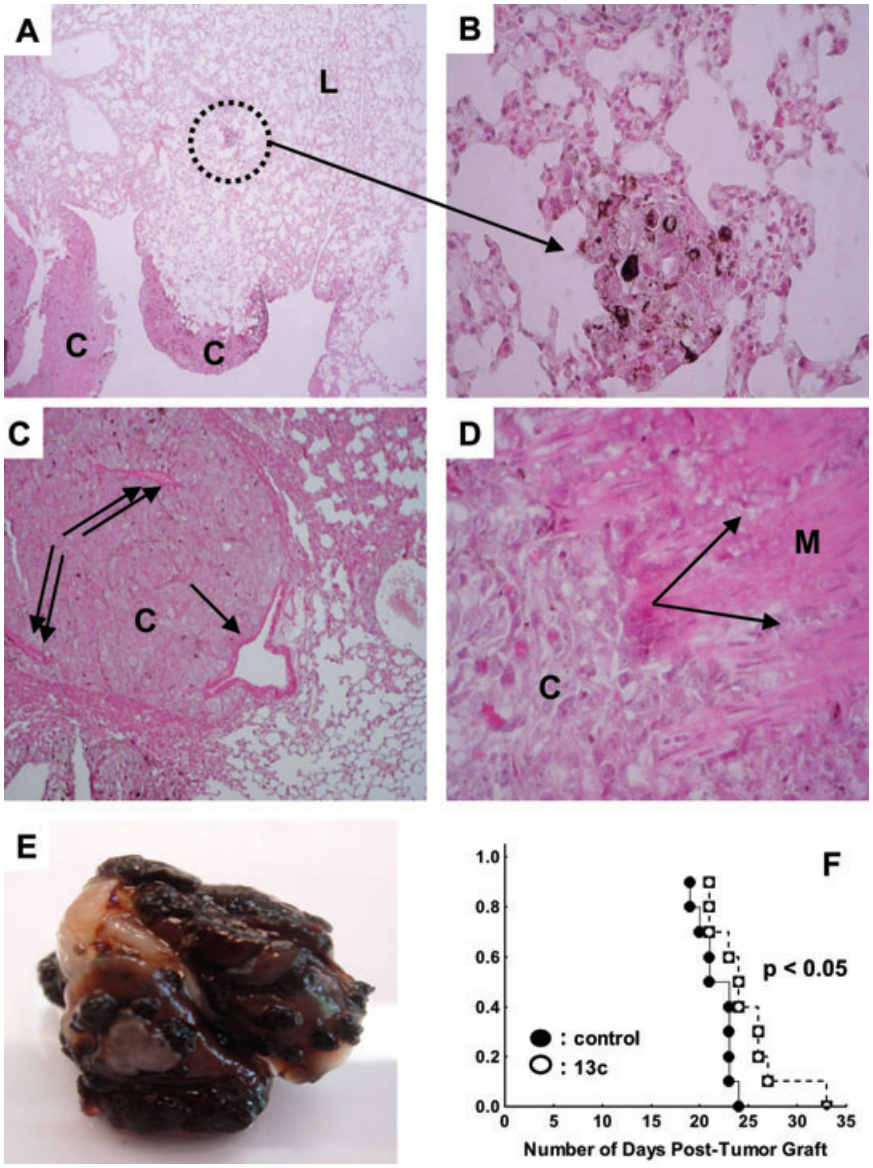

Fig. 8 Characterization of the *in vivo* anticancer activity of **13c** in the mouse B16F10 pseudometastatic lung model. (**A**, G×40 and **B**, G×200) Illustrations of B16F10 cancer development in the mouse lungs five days after B16F10 melanoma cells i.v. injection into the tail veins of the mice. (**C**) Major B16F10 cancer development is present 3 weeks post-tumour cell injection with obstructive processes of major lung airways (see the double arrows). The single arrow points to a major lung airway not yet obstructed by cancer development. (**D**) Marked invasive processes from the cancer C bulk to and through the peritoneal muscle wall M are also observed for this B16F10 melanoma model. (**E**) The lungs are almost completely destroyed by the melanoma by the third week after the tumour grafting procedure. (**F**) B16F10 melanoma pulmonary pseudo metastases were obtained by the i.v. (lateral tail vein) administration of 2.5×10^5 B16F10 cells (200 μl). Mice were randomized on the fourth day post-tumour grafting, and treatments began the next day. Each experimental group included 11 mice. Compound **13c** (40 mg/kg) was administered directly to the lungs (50 μl of suspension for inhalation at 1.6% compound **13c** (m/v) by the endotracheal route) three times (Monday, Wednesday and Friday) a week for three consecutive weeks. Control mice were treated exactly as **13c**-treated mice but without receiving **13c**.

13c is p53 independent and thus probably not due to DNA damage as clearly suggested by the quantitative videomicroscopy (Fig. 2) and kinase (Fig. 5) analyses.

These data must then be analysed in a broader context in parallel with those reported in Table 1, which indicate that **13c** displays similar *in vitro* growth inhibitory activity in cancer cells that possess various levels of resistance to pro-apoptotic stimuli (including U373 [37], A549 [36] and VM48 [38] cell lines) and in cancer cells that are actually sensitive to pro-apoptotic stimuli such as Hs683 oligodendroglioma [37] and the VM21 [38] cells. In addition, the A549 cell line displays multiple types of chemoresistance, including the overexpression of cyclooxygenase-2 (COX-2) [39], prostaglandin E synthetase (PGES) [39], ornithine decarboxylase (ODC) [39], LRP [39], glutathione-*S*-transferases [39], and ABCC1 [36], ABCC2 [36] and ABCG2 [36] MDR-related pumps; it does not display higher resistance to **13c** than the other cancer cell lines under study (Table 1).

As a proof of concept, we used the B16F10 melanoma pseudometastatic lung model [20, 21] to investigate whether **13c** without any specific formulation displays significant *in vivo* anticancer activity. Although compound **13c** inhibited the activity of various kinases implicated in a broad range of cancers, we first wanted to target lung cancers because this compound is active not only on wild-type forms of EGFR but also on various mutated forms, such as those encountered in NSCLCs. The **13c** trivanillate possesses several ester moieties (Fig. 1), and it will be therefore

rapidly destroyed by esterases if administered through systemic i.v. or oral routes. Compound **13c** has thus been administered in *vivo* through an inhalation-related procedure that we described recently [21]. Inhalation procedures avoid systemic or oral routes of administration and allow direct concentration of an anticancer compound of interest to the target, that is the lung cancer into the lungs [21]. In this study, we observed significant *in vivo* anticancer activity for compound **13c** in the aggressive B16F10 lung pseudometastatic model (Fig. 8F). Clear evidence of B16F10 cancer development in the lungs is already present five days after B16F10 melanoma cell i.v. injection into the tail veins of the mice (Fig. 8A and B). Major cancer development is present 3 weeks post-tumour cell injection with obstructive processes of major lung airways (see the double arrows in Fig. 8C) and marked invasive processes through the peritoneal muscle wall (Fig. 8D). The lungs are virtually destroyed by the melanoma 3 weeks after this tumour grafting procedure (Fig. 8E).

Discussion

Of the three trivanillates under study, **13a** appeared to be cytotoxic, as did the reference compound curcumin, while **13b** and **13c** appeared to be cytostatic (Fig. 2). The cytotoxic effects of **13a** were not related to pro-apoptotic effects (Fig. 3), anti-kinase activity (Fig. 4) or modifications of $[Ca^{2+}]_i$ (Fig. 6). These features are in contrast with the cytotoxic effects of curcumin that relate to the disruption of the mammalian target of the rapamycin–raptor complex [40] and calcium homeostasis, a feature that in turn induces programmed cell death [41] as also observed in the current study (Fig. 3). Resveratrol also induces apoptosis through impairments of calcium homeostasis [19]. The three trivanillates under study displayed markedly distinct modifications of $[Ca^{2+}]_i$. In fact, **13a** did not modify $[Ca^{2+}]_i$, while **13b** and **13c** induced a transient and a sustained increase in $[Ca^{2+}]_i$, respectively (Fig. 4). Although it has already been demonstrated that EGCG increases $[Ca^{2+}]_i$ in cancer cells mainly due to influx of extracellular calcium and partly due to release of intracellular stores [18], the current data clearly show that **13b** and **13c** increased $[Ca^{2+}]_i$ through the release of calcium from the endoplasmic reticulum and not from an influx of extracellular calcium (Fig. 6).

The chemical substitution of three OMe groups in **13a** by three F groups in **13b** (Fig. 1A) brought about weak anti-kinase effects (Fig. 4) and transient modifications in $[Ca^{2+}]_i$ (Fig. 6) and converted **13b** from a cytotoxic compound into a cytostatic one (Fig. 2) without significant modifications of its *in vitro* growth inhibitory activity (Table 1). Then, the chemical substitution of three F groups in **13b** by three Cl groups in **13c** (Fig. 1) brought about potent anti-kinase effects (Fig. 4) and sustained modifications of $[Ca^{2+}]_i$ (Fig. 6) without altering the cytostatic profile of the compound (Fig. 2).

This study then demonstrated that compound **13c** displays similar growth inhibitory activity in wild-type *versus* p53-deficient cancer cells (Fig. 7), a feature that perfectly fits with our previous data, which clearly indicated that this compound displays similar growth inhibitory effects in cancer cell lines that exhibit various levels of resistance or sensitivity to pro-apoptotic stimuli [2]. In addition, the data from the present study showed that the trivanillate **13c** is not a substrate in various MDR models and that it is active against cisplatin-resistant cancer cells (Fig. 7), remembering that cisplatin is widely used to treat NSCLC patients and that NSCLC patients rapidly develop resistance to cisplatin. We aim to further investigate the therapeutic benefits that would be contributed by **13c** in various lung cancer models because this compound is active not only on wild-type forms of EGFR but also on various mutated forms, such as those encountered in NSCLCs, as detailed later.

The fact that compound **13c** does not appear to be an MDR substrate is an important feature because in addition to protein kinase inhibitor (PKI) resistance based on altered target structures, the active removal of these therapeutic agents by the MDR-ABC transporters should also be considered as a major cause of clinical resistance to PKIs [42].

It is well known that $[Ca^{2+}]_i$ modifications lead to marked modifications in actin cytoskeleton organization [43, 44], a feature that we indeed observed in this study (Fig. 5), and in turn, actin-binding proteins influence Ca^{2+} signalling [45, 46]. Actin cytoskeleton organization is also under the control of a large set of kinases [47–49]. Although 2 μM **13c**, which represents ~5% of the median IC_{50} of **13c** in 12 distinct cancer cell lines (Table 1), displayed modest effects on $[Ca^{2+}]_i$ (Fig. 6), this concentration inhibited the activity of 26 kinases by >75% (Fig. 4). The anti-kinase activity associated with compound **13c** as reported here places it among the most potent anti-kinase polyphenolic compounds described heretofore [13]. Of the 26 kinases targeted by **13c** at a low concentration, eight of these kinases (*Yes*, *Fyn*, FGF-R1, EGFR, *Btk*, *Mink*, *Ret* and *Itk*) are directly implicated in the control of actin cytoskeleton organization (Fig. 5). An additional set of six kinases also implicated in the control of the actin cytoskeleton were also inhibited by 50–75% following treatment with 2 μM **13c** (Fig. 4). These six kinases are *Kit*, *Pak3*, *Apha3*, *Syk*, *Erk6* (p38-gamma) and PKA.

Among the **13c**-targeted kinases implicated in the control of the actin cytoskeleton are various members of the *Src* family-tyrosine kinase (SFK) proteins (including *Src*, *Yes* and *Fyn*), FGF-R1 and EGFR, which are also dependent on *Src* to control actin cytoskeleton organization, *Fes*, *Fer*, *Btk*, *Mink*, *Ret* and *Itk*.

Most, if not all, **13c**-targeted kinases (Fig. 4) are overexpressed in a wide range of cancers, such as *Mertk* [50] and *Mink1* [51] in various types of cancers, MAP4K4 in pancreatic cancer [52], *Ret* in medullary thyroid carcinoma [53], TRK-B in gliomas [54], *Flt-3* in leukemia [55], *Btk* in lymphoma [56] and *Syk* in peripheral T cell lymphoma [57].

Three subgroups of kinases targeted by **13c** are particularly noteworthy.

The first subgroup relates to SFKs that include nine enzymes with homology to *Src* [58]. High levels of *Src* activity are found in a broad spectrum of cancers [59] and it was recently suggested that increased SFK protein levels, and more importantly SFK

tyrosine kinase activity, are linked to cancer progression and metastatic disease by facilitating the action of other signalling proteins [58]. Compound **13c** markedly decreased the activity of four SFKs, *Fyn*, *Yes*, *Lyn* and *Matk* (Fig. 4).

The second subgroup of **13c**-related targets includes kinases implicated in angiogenesis. Thus, compound **13c** decreased both *Fes* and *Fer* kinase activities (Fig. 4), both of which are the only known members of a distinct subfamily of the non-receptor PTK family [60]. These two kinases have roles in regulating cytoskeletal rearrangements and inside-out signalling that accompany receptor–ligand, cell–matrix and cell–cell interactions [60]. **13c**-induced cytostatic effects on cancer cells could therefore be partly explained through **13c**-induced inhibition of *Fer* and *Fes* kinase activities.

The third subgroup of **13c**-related targets includes members of the epidermal growth factor receptor (EGFR) family, which have been implicated in pathophysiology of various cancers, including NSCLC [61, 62]. The data from this study clearly showed that compound **13c** displays potent inhibitory activity (at ~5% of its IC_{50}) against EGFR, including not only the wild-type form but also the L858R and/or T790M mutated forms. These data thus prompted us to investigate the anticancer activity of **13c** *in vivo* in lung cancers. Our choice of targeting lung cancer through the inhalation route and not through conventional i.v. or oral ones was influenced by the fact that **13c** displays three ester bounds that will not resist *in vivo* esterases through systemic or oral administration. In addition, very subtle modifications of the chemical backbone of these trivanillates markedly changed their anti-kinase profiles (Fig. 4) and converted a cytotoxic trivanillate without anti-kinase activity (**13a**; Fig. 2) into cytostatic moieties (**13b** and **13c**; Figs 2 and 3) and induced marked anti-kinase activity for **13c** (Fig. 4). We thus decided not to modify compound **13c** at the chemical level with the aim of reinforcing it against esterases (*e.g.* ester substitution with amides) to maintain its anti-kinase profile. We observed that **13c** contributed weak but nevertheless significant therapeutic benefits in a particularly aggressive model of lung pseudometastasis (Fig. 8). We are currently developing dry powder-related formulations for **13c** to significantly improve its *in vivo* anticancer activity with respect to lung cancers. In regard of the definition of solubility in the European Pharmacopeia (7.0), compound **13c** is practically non-soluble in water but the preliminary data we already obtained demonstrate that it is soluble in a mixture of dichloromethane and ethanol (50:50, v/v). Mixtures of dichloromethane and ethanol are usually employed to solubilize phospholipids and lipids when elaborating liposomes that are vectors, which mimic the cell membrane. It thus seems that **13c** could be more soluble in the cellular membrane components than in the aqueous ones. In addition, while the ester moieties of **13c** could be hydrolyzed by esterases in the systemic circulation and metabolized in the liver, these enzymatic metabolisms are less developed in the lungs [63]. Indeed, most of enzymes that are present in the liver are also present in the lungs but in 5–20 less extent [63]. Moreover, the toxic side effects, which could appear through the systemic route with a multi-anti-kinase compound such as **13c**, could be attenuated through the inhalation route. We are currently developing various types of formulations with 13c dry powders embedded in cyclodextrins, liposomes or polymeric and/or lipid nanoparticles.

NSCLCs are the leading cause of cancer death in the world [3] and great hopes rest in the use of anti-EGFR compounds [61, 62]. Indeed, activating mutations in the form of deletions of exon 19 (del 19) or the missense mutation L858R in the EGFR TK domain predict outcome to EGFR TKIs such as gefitinib and erlotinib [64, 65]. Pooled data from several phase II studies show that gefitinib and erlotinib induce responses in over 70% of NSCLC patients harbouring EGFR mutations, with progression-free survival ranging from 9 to 13 months and median survival of approximately 23 months [65]. However, the secondary T790M mutation confers resistance to EGFR TKIs, and the presence of double mutations (T790M plus either L858R or del 19) at the time of diagnosis could be much more frequent than originally thought [65].

In conclusion, specific trivanillates belonging to the polyphenolic group of compounds could be used to combat cancer cells that display acquired resistance to targeted agents, intrinsic resistance to apoptosis, the MDR phenotype and/or kinase inhibitors, including mutated forms of EGFR. This study shows that compound **13c**, a tri-chloride trivanillic ester, displays marked inhibitory activities against more than 20 kinases and that this pan-anti-kinase activity occurs below one-tenth of its mean IC_{50} *in vitro* toward a panel of 12 cancer cell lines. About half of the kinases targeted by **13c** are implicated in the control of actin cytoskeleton organization to some degree, and this compound accordingly impairs actin cytoskeleton organization and reveals itself to be a cytostatic, rather than cytotoxic, compound that impairs mitosis. All of these features concomitantly occur with calcium homeostasis impairment but without provoking MDR phenotype activation. The anticancer properties associated with **13c** enabled this compound to contribute therapeutic benefits *in vivo* in a mouse melanoma pseudometastatic lung model. These data thus argue in favour of further chemically modifying trivanillates to produce novel and potent anticancer drugs.

Conflict of Interest

The authors confirm that there are no conflicts of interest.

Supporting Information

Additional Supporting Information may be found in the online version of this article.

Fig. SI-1 Morphological illustrations of the cytostatic effects provoked by **6b** on U373 cells.

Fig. SI-2 Effects of **13a**, **13b** and **13c** compounds on cytosolic ($[Ca^{2+}]_i$) of free Ca^{2+} without $[Ca^{2+}]_e$.

Fig. SI-3 Characterization of the *in vitro* anticancer activity of **13c** in various MDR cancer cell lines.

Table SI-1 List of kinases and substrates.

Please note: Wiley-Blackwell is not responsible for the content or functionality of any supporting materials supplied by the authors. Any queries (other than missing material) should be directed to the corresponding author for the article.

References

1. **Simpson CD, Anyiwe K, Schimmer AD.** Anoikis resistance and tumour metastasis. *Cancer Lett*. 2008; 272: 177–85.
2. **Lamoral-Theys D, Pottier L, Kerff F, *et al.*** Simple di- and trivanillates exhibit cytostatic properties toward cancer cells resistant to pro-apoptotic stimuli. *BioOrg Med Chem*. 2010; 18: 3823–33.
3. **Han S, Roman J.** Targeting apoptotic signalling pathways in human lung cancer. *Curr Cancer Drug Targets*. 2010; 10: 566–74.
4. **Soengas MS, Lowe SW.** Apoptosis and melanoma chemoresistance. *Oncogene*. 2003; 22: 3138–51.
5. **Wong HH, Lemoine NR.** Pancreatic cancer: molecular pathogenesis and new therapeutic targets. *Nat. Rev. Gastroenterol Hepatol*. 2009; 6: 412–22.
6. **D'Amico TA, Harpole DH Jr.** Molecular biology of esophageal cancer. *Chest Surg Clin N Am*. 2000; 10: 451–69.
7. **Lefranc F, Brotchi J, Kiss R.** Possible future issues in the treatment of glioblastomas, with a special emphasis on cell migration and the resistance of migrating glioblastoma cells to apoptosis. *J Clin Oncol*. 2005; 23: 2411–22.
8. **Anuchapreeda S, Leechanachai P, Smith MM, *et al.*** Modulation of P-glycoprotein expression and function by curcumin in multidrug-resistant human KB cells. *Biochem Pharmacol*. 2002; 64: 573–82.
9. **Mayur YC, Peters GJ, Prasad VV, *et al.*** Design of new drug molecules to be used in reversing multidrug resistance in cancer cells. *Curr Cancer Drug Targets*. 2009; 9: 298–306.
10. **Gossage L, Eisen T.** Targeting multiple kinase pathways: a change in paradigm. *Clin Cancer Res*. 2010; 16: 1973–8.
11. **Knight ZA, Lin H, Shokat KM.** Targeting the cancer kinome through polypharmacology. *Nat Rev Cancer*. 2010; 10: 130–7.
12. **Fedorov O, MIler S, Knapp S.** The (un)target cancer kinome. *Nat Chem Biol*. 2010; 6: 166–9.
13. **Lamoral-Theys D, Pottier L, Dufrasne F, *et al.*** Natural polyphenols that display anticancer properties through inhibition of kinase activity. *Curr Med Chem*. 2010; 17: 812–25.
14. **Bar-Sela G, Epelbaum R, Schaffer M.** Curcumin as an anti-cancer agent: review of the gap between basic and clinical applications. *Curr Med Chem*. 2010; 17: 190–7.
15. **Kraft TE, Parisotto D, Schempp C, *et al.*** Fighting cancer with red wine? Molecular mechanisms of resveratrol. *Crit Rev Food Sci Nutr*. 2009; 49: 782–99.
16. **Butt MS, Sultan MT.** Green tea: nature's defense against malignancies. *Crit Rev Food Sci Nutr*. 2009; 49: 463–73.
17. **Martin S, Giannone G, Andriantsitohaina R, *et al.*** Delphinidin, an active compound of red wine, inhibits endothelial cell apoptosis *via* nitric oxide pathway and regulation of calcium homeostasis. *Br J Pharmacol*. 2003; 139: 1095–102.
18. **Kim HJ, Yum KS, Sung JH, *et al.*** Epigallocatechin-3-gallate increases intracellular [Ca^{2+}] in U87 cells mainly by influx of extracellular Ca^{2+} and partly by release of intracellular stores. *Naunyn Schmiedebergs Arch Pharmacol*. 2004; 369: 260–7.
19. **Sareen D, Darjatmoko SR, Albert DM, *et al.*** Mitochondria, calcium, and calpain are key mediators of resveratrol-induced apoptosis in breast cancer. *Mol Pharmacol*. 2007; 72: 1466–75.
20. **Mathieu V, Le Mercier M, De Neve N, *et al.*** Galectin-1 knockdown increases sensitivity to temozolomide in a B16F10 mouse metastatic melanoma model. *J Invest Dermatol*. 2007; 127: 2399–410.
21. **Wauthoz N, Deleuze P, Hecq J, *et al.*** *In vivo* assessment of temozolomide local delivery for lung cancer inhalation therapy. *Eur J Pharm Sci*. 2010; 39: 402–11.
22. **Lefranc F, Facchini V, Kiss R.** Pro-autophagic drugs: a novel means to combat apoptosis-resistant cancers, with a special emphasis on glioblastomas. *Oncologist* 2007; 12: 1395–403.
23. **Mathieu V, Pirker C, Martin de Lassalle E, *et al.*** The sodium pumpa alpha-1 subunit: a disease progression-related target for metastatic melanoma treatment. *J Cell Mol Med*. 2009; 13: 3960–72.
24. **Shen DW, Cardarelli C, Hwang J, *et al.*** Multiple drug-resistant human KB carcinoma cells independently selected for high-level resistance to colchicine, adriamycin, or vinblastine show changes in expression of specific proteins. *J Biol Chem*. 1986; 261: 7762–70.
25. **Heffeter P, Jakupec MA, Korner W, *et al.*** Multidrug-resistant cancer cells are preferential targets of the new antineoplastic lanthanum compound KP772 (FFC24). *Biochem Pharmacol*. 2007; 73: 1873–86.
26. **Yen Y, Grill SP, Dutschman GE, *et al.*** Characterization of a hydroxyurea-resistant human KB cell line with supersensitivity to 6-thioguanine. *Cancer Res*. 1994; 54: 3686–91.
27. **Zijlstra JG, de Vries EG, Mulder NH.** Multifactorial drug resistance in an adriamycin-resistant human small cell lung carcinoma cell line. *Cancer Res*. 1987; 47: 1780–4.
28. **Bunz F, Fauth C, Speicher MR, *et al.*** Targeted inactivation of p53 in human cells does not result in aneuploidy. *Cancer Res*. 2002; 62: 1129–33.
29. **Janson V, Andersson B, Behnam-Motlagh P, *et al.*** Acquisition of cisplatin-resistance in malignant mesothelioma cells abrogates Na^+, K^+, 2Cl(−)-cotransport activity and cisplatin-induced early membrane blebbing. *Cell Physiol Biochem*. 2008; 22: 45–56.
30. **Yanovich S, Hall RE, Weinert C.** Resistance to natural killer cell-mediated cytolysis by a pleiotropic drug-resistant human erythroleukemia (K562-R) cell line. *Cancer Res*. 1986; 46: 4511–5.
31. **Mégalizzi V, Mathieu V, Mijatovic T, *et al.*** 4-IBP: a sigma-1 receptor agonist decreases the migration of human cancer cells including glioblastoma cells *in vitro* and sensitizes them *in vitro* and *in vivo* to the cytotoxic insults of pro-apoptotic and pro-autophagic drugs. *Neoplasia*. 2007; 9: 358–69.
32. **Debeir O, Mégalizzi V, Warzée N, *et al.*** Videomicroscopic extraction of specific information on cell proliferation and migration *in vitro*. *Exp Cell Res*. 2008; 314: 2985–98.

33. **Gailly P, Hermans E, Gillis JM.** Role of $[Ca^{2+}](i)$ in 'Ca^{2+} stores depletion-Ca^{2+} entry coupling' in fibroblasts expressing the rat neurotensin receptor. *J Physiol*. 1996; 491: 635–46.
34. **Palmer AE, Jin C, Reed JC, *et al.*** Bcl-2-mediated alterations in endoplasmic reticulum Ca^{2+} analyzed with an improved genetically encoded fluorescent sensor. *Proc Natl Acad Sci USA* 2004; 101: 17404–9.
35. **Pigozzi D, Ducret T, Tajeddine N, *et al.*** Calcium store contents control the expression of TRPC1, TRPC3 and TRPV6 proteins in LNCaP prostate cancer cell line. *Cell Calcium*. 2006; 39: 401–15.
36. **Mijatovic T, Jungwirth U, Heffeter P, *et al.*** The Na+/K+-ATPase is the Achilles Heel of multidrug resistant cancer cells. *Cancer Lett*. 2009; 282: 30–4.
37. **Ingrassia L, Lefranc F, Dewelle J, *et al.*** Structure-activity-relationship analysis of novel derivatives of narciclasine (an Amaryllidaceae Isocarbostyril alkaloid) as potential anti-cancer agents. *J Med Chem*. 2009; 52: 1100–4.
38. **Van Goietsenoven G, Hutton J, Becker JP, *et al.*** Targeting of eEF1A with Amaryllidaceae isocarbostyrils as a strategy to combat melanomas. *FASEB J*. 2010; 24: 4575–84.
39. **Mathieu A, Remmelink M, D'Haene N, *et al.*** Development of a chemoresistant orthotopic human nonsmall cell lung carcinoma model in nude mice. *Cancer*. 2004; 101: 1908–18.
40. **Beevers CS, Chen L, Liu L, *et al.*** Curcumin disrupts the mammalian target of rapamycin-raptor complex. *Cancer Res*. 2009; 69: 1000–8.
41. **Das R, Roy A, Dutta N, *et al.*** Reactive oxygen species and imbalance of calcium homeostasis contributes to curcumin induced programmed cell death in Leishmania donovani. *Apoptosis*. 2008; 13: 867–82.
42. **Hegedus C, Ozvegy-Laczka C, Szakacs G, *et al.*** Interaction of ABC multidrug transporters with anticancer protein kinase inhibitors: substrates and/or inhibitors? *Curr Cancer Drug Targets*. 2009; 9: 252–72.
43. **Oertner TG, Matus A.** Calcium regulation of actin dynamics in dendritic spines. *Cell Calcium*. 2005; 37: 477–82.
44. **Lange K, Gartzke J.** F-actin-based Ca signaling—a critical comparison with the current concept of Ca signaling. *J Cell Physiol*. 2006; 209: 270–87.
45. **Santella L, Puppo A, Chun JT.** The role of the actin cytoskeleton in calcium signaling in starfish oocytes. *Int J Dev Biol*. 2008; 52: 571–84.
46. **Chun JT, Santella L.** Roles of the actin-binding proteins in intracellular Ca^{2+} signaling. *Acta Physiol*. 2009; 195: 61–70.
47. **Olson MF.** Applications for ROCK kinase inhibition. *Curr Opin Cell Biol*. 2008; 20: 242–8.
48. **Matenia D, Mandelkow EM.** The tau of MARK: a polarized view of the cytoskeleton. *Trends Biochem Sci*. 2009; 34: 332–42.
49. **Wells CM, Jones GE.** The emerging importance of group II PAKs. *Biochem J*. 2010; 425: 465–73.
50. **Hafizi S, Dahlbäck B.** Signaling and functional diversity within the Axl subfamily of receptor tyrosine kinases. *Cytokine Growth Factor Rev*. 2006; 17: 295–304.
51. **Hu Y, Leo C, Yu S, *et al.*** Identification and functional characterization of a novel human misshapen/Nck interacting kinase-related kinase, hMINK beta. *J Biol Chem*. 2004; 279: 54387–97.
52. **Badea L, Herlea V, Dima SO, *et al.*** Combined gene expression analysis of whole-tissue and microdissected pancreatic ductal adenocarcinoma identifies genes specifically overexpressed in tumour epithelia. *Hepatogastroenterology*. 2008; 55: 2016–27.
53. **Santarpia L, Ye L, Gagel RF.** Beyond RET: potential therapeutic approaches for advanced and metastatic medullary thyroid carcinoma. *J Intern Med*. 2009; 266: 99–113.
54. **Wadhwa S, Nag TC, Jindal A, *et al.*** Expression of the neurotrophin receptors Trk A and Trk B in adult human astrocytomas and glioblastoma. *J Biosci*. 2003; 28: 181–8.
55. **Sanz M, Burnett A, Lo-Coco F, *et al.*** FLT3 inhibition as a targeted therapy for acute myeloid leukemia. *Curr Opin Oncol*. 2009; 21: 594–600.
56. **Pan Z.** Bruton's tyrosine kinase as a drug discovery target. *Drug News Perspect*. 2008; 21: 357–62.
57. **Feldman AL, Sun DX, Law ME, *et al.*** Overexpression of Syk tyrosine kinase in peripheral T-cell lymphomas. *Leukemia*. 2008; 22: 1139–43.
58. **Wheeler DL, Iida M, Dunn EF.** The role of Src in solid tumours. *Oncologist*. 2009; 14: 667–78.
59. **Martin GS.** The hunting of the Src. *Nat Rev Mol Cell Biol*. 2001; 2: 467–75.
60. **Greer P.** Closing in on the biological functions of Fps/Fes and Fer. *Nat Rev Cell Biol*. 2002; 3: 278–89.
61. **Gazdar AF.** Activating and resistance mutations of EGFR in non-small-cell lung cancer: role in clinical response to EGFR tyrosine kinase inhibitors. *Oncogene*. 2009; 28: S24–31.
62. **Costa DB, Nguyen KS, Cho BC, *et al.*** Effects of erlotinib in EGFR mutated non-small cell lung cancers with resistance to gefitinib. *Clin Cancer Res*. 2008; 14: 7060–7.
63. **Labiris NR, Dolovich MB.** Pulmonary drug delivery. Part I: Physiological factors affecting therapeutic effectiveness of aerosolized medications. *J Clin Pharmacol*. 2003; 56: 588–99.
64. **John T, Liu G, Tsao MS.** Overview of molecular testing in non-small-cell lung cancer: mutational analysis, gene copy number, protein expression and other biomarkers of EGFR for the prediction of response to tyrosine kinase inhibitors. *Oncogene*. 2009; 28: S14–23.
65. **Rosell R, Moran T, Carcereny E, *et al.*** Non-small-cell lung cancer harbouring mutations in the EGFR kinase domain. *Clin Transl Oncol*. 2010; 12: 75–80.